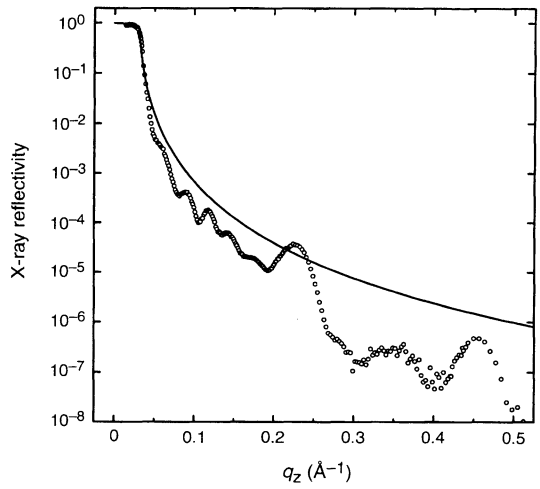

FIG. 3 X-ray reflectivity (measured at beamline X22B at the National Synchrotron Light Source) versus q_z for a self-replicating eight-layer film on Si prepared as the films of Fig. 2 (circles). (q_z is the wavevector transfer along the surface normal.) The reflectivity decreases faster at large q_z than that of a perfectly flat Si interface (Fresnel theory, solid line), indicating a substantial substrate roughness of the order of 5 Å. Oscillations in the reflectivity are due to the interference between rays reflected from the top and bottom of the film. The existence of multiple oscillations shows the presence of well ordered layers. The total film thickness derived from the 0.028 Å^{-1} spacing of these Kiessig fringes is 224 ± 8 Å. The quasi-Bragg peaks at ~0.23 and ~0.45 Å^{-1} indicate a layer spacing of 28 Å, close to the expected thickness of an untilted OTS monolayer[20]. Thus, the ratio of the total thickness to the layer spacing (8.0 ± 0.3) confirms the existence of eight silane layers, in accordance with the self-replicating growth model. The broad, weaker peak at ~0.36 Å^{-1} originates from the presence of the OTS bilayers (Fig. 1) and is absent in the reflectivity of NTS films with same number of layers grown layer-by-layer (not shown)[20]. The reflectivity results for a four-layer film show that the thickness is half that of the eight-layer film; but a detailed interpretation is slightly complicated by the fact that, for technical reasons, the quasi-Bragg peak is far less pronounced, and so the data are not shown here.

from the copy[29]) is achieved with conservation of the overall structural integrity of the system, which leads to the growth of a three-dimensional structure (multilayer), starting from an initial two-dimensional nucleus (monolayer) itself generated via controlled self-assembly at the interface. Thus, unlike the related self-multiplication previously observed in some layer silicates[27], the present process does not rely on the availability of a template of natural origin. Our system contains the instructions required for its own replication while still offering the advantage that the replication is discontinuous and subject to precise control through an external chemical trigger operation. □

Received 11 June; accepted 8 October 1996.

1. Ulman, A. *An Introduction to Ultrathin Organic Films From Langmuir-Blodgett to Self-Assembly* (Academic, Boston, 1991).
2. Kuhn, H. & Möbius, D. in *Physical Methods of Chemistry* (eds Rossiter, B. W. & Baetzold, R. C.) 375–542 (Wiley, New York, 1993).
3. Maoz, R., Netzer, L., Gun, J. & Sagiv, J. *J. Chim. Phys.* **85,** 1059–1065 (1988).
4. Keller, S. W., Kim, H.-N. & Mallouk, T. E. *J. Am. Chem. Soc.* **116,** 8817–8818 (1994).
5. Thompson, M. E. *Chem. Mater.* **6,** 1168–1175 (1994).
6. Byrd, H. *et al. J. Am. Chem. Soc.* **116,** 295–301 (1994).
7. Decher, G., Hong, J.-D., Lowack, K., Lvov, Y. & Schmitt, J. in *Self-Production of Supramolecular Structures From Synthetic Structures to Models of Minimal Living Systems* (eds Fleischaker, G. R., Colonna, S. & Luisi, P. L.) 267–272 (NATO ASI Ser. C. Vol. 446, Kluwer Academic, Dordrecht, 1994).
8. Li, D.-Q. *et al. J. Am. Chem. Soc.* **112,** 7389–7390 (1990).
9. Ogawa, K., Mino, N., Tamura, H. & Hatada, M. *Langmuir* **6,** 851–856 (1990).
10. Cairns-Smith, A. G. *Genetic Takeover and the Mineral Origins of Life* (Cambridge Univ. Press, 1982).
11. Orgel, L. E. *Nature* **358,** 203–209 (1992).
12. *Self-Production of Supramolecular Structures From Synthetic Structures to Models of Minimal Living Systems* (eds Fleischaker, G. R., Colonna, S. & Luisi, P. L.) (NATO ASI Ser. C. Vol. 446, Kluwer Academic, Dordrecht, 1994).
13. Kuhn, H. & Waser, J. in *The Lock-and-Key Principle The State of the Art—100 Years On* (ed. Behr, J.-P.) 247–306 (Wiley, Chichester, 1994).
14. Lehn, J.-M. *Angew. Chem. Int. Edn. Engl.* **29,** 1304–1319 (1990).
15. Whitesides, G. M., Mathias, J. P. & Seto, C. T. *Science* **254,** 1312–1319 (1991).
16. Müller, W. *et al. Science* **262,** 1706–1708 (1993).
17. Fuhrhop, J.-H. & Krull, M. in *Frontiers in Supramolecular Organic Chemistry and Photochemistry* (eds Schneider, H.-J. & Dürr, H.) 223–249 (VCH, Weinheim, 1991).
18. Ozin, G. A. *Adv. Mater.* **4,** 612–649 (1992).
19. Maoz, R., Yam, R., Berkovic, G. & Sagiv, J. in *Thin Films* Vol. 20 (ed. Ulman, A.) 41–68 (Academic, San Diego, 1995).
20. Maoz, R., Sagiv, J., Degenhardt, D., Möhwald, H. & Quint, P. *Supramol. Sci.* **2,** 9–24 (1995).
21. Casal, H., Cameron, D. G. & Mantsch, H. *Can. J. Chem.* **61,** 1736–1742 (1983).
22. Jones, R. N., McKay, A. F. & Sinclair, R. G. *J. Am. Chem. Soc.* **74,** 2575–2578 (1952).
23. Nuzzo, R. G., Dubois, L. H. & Allara, D. L. *J. Am. Chem. Soc.* **112,** 558–569 (1990).
24. Andrianov, K. A. & Izmaylov, B. A. *J. Organomet. Chem.* **8,** 435–450 (1967).
25. Maoz, R. & Sagiv, J. *J. Colloid Interface Sci.* **100,** 465–496 (1984).
26. Parikh, A. N., Allara, D. L., Ben Azouz, I. & Rondelez, F. *J. Phys. Chem.* **98,** 7577–7590 (1994).
27. Weiss, A. *Angew. Chem. Int. Edn Engl.* **20,** 850–860 (1981).
28. Bachmann, P. A., Luisi, P. L. & Lang, J. *Nature* **357,** 57–59 (1992).
29. Fleischaker, G. R. in *Self-Production of Supramolecular Structures From Synthetic Structures to Models of Minimal Living Systems* (eds Fleischaker, G. R., Colonna, S. & Luisi, P. L.) 33–41 (NATO ASI ser. C. Vol. 446, Kluwer Academic, Dordrecht, 1994).

ACKNOWLEDGEMENTS. We thank K. Ogawa of Matsushita Co. (Kyoto) for supplying the NTS material. This work was supported by the MINERVA Foundation, Munich, Germany and the Philip M. Klutznick Fund for Research at the Weizmann Institute. Brookhaven National Laboratory is supported by the US DOE.

CORRESPONDENCE and requests for materials should be addressed to J.S. (e-mail: bpherut@weizmann.weizmann.ac.il).

Effect of slab temperature on deep-earthquake aftershock productivity and magnitude–frequency relations

Douglas A. Wiens & Hersh J. Gilbert

Department of Earth and Planetary Sciences, Washington University, St Louis, Missouri 63130, USA

DEEP earthquakes generally show fewer aftershocks and a larger variability in magnitude–frequency relations than shallow earthquakes[1–5]. These characteristics and the factors that control them may place constraints on the mechanism of deep earthquakes, which is still uncertain[6–8]. Here we show that systematic variations in aftershock productivity and magnitude–frequency relations are related to the temperature of the downgoing slab, as inferred from the vertical velocity and age of the subducting lithosphere. Deep earthquakes with substantial aftershock sequences are found only in colder slabs, and earthquakes in warmer slabs consistently show few aftershocks. Magnitude–frequency relations for deep earthquakes also show systematic variations as a function of slab thermal structure, with warmer slabs showing fewer small earthquakes (lower '*b*-values'). The statistical properties of deep earthquakes thus appear to be temperature sensitive to an extent not observed for shallow earthquakes, and not adequately explained by simple geometrical limitations on fault width.

The aftershock productivity of deep earthquakes varies from a nearly complete absence of aftershocks to aftershock rates approaching those of typical shallow earthquakes. As extreme examples, the 1970 Colombia deep earthquake (moment magnitude $M_w = 8.0$) produced no reported aftershocks, whereas 144 aftershocks have recently been recorded for the much smaller 9 March 1994 Tonga event ($M_w = 7.6$)[9,10].

To address the systematics of deep-earthquake aftershock production, we have compiled two datasets. One dataset consists of all 1958–96 deep earthquakes with $M_w \geq 7.0$ (Table 1*a*). For this dataset we compiled all reported aftershocks with body wave

magnitude (m_b) ≥ 4.5 with the magnitude threshold imposed to reduce the effect of uneven detection levels. Events are counted as aftershocks if they occurred within 100 km of the mainshock hypocentre within a period of 3 months following the mainshock. For most cases, this simple criterion readily distinguishes aftershocks from the background seismicity, particularly because most deep seismic zones show relatively low seismicity levels. For a few active deep zones, seismicity rates are high enough that this criterion might include several randomly occurring background events. In these cases, the time window is limited to the period in which the seismicity rate exceeds the background seismicity rate.

We also compiled a second dataset to take advantage of the superior instrumentation available for recent deep earthquakes. This dataset consists of 1990–96 deep earthquakes with $M_w \geq 6.0$, for which waveform data is available from at least one station within 12° distance (Table 1*b*). For the 1994 Tonga and Bolivia events we used results from temporary networks operating in these regions[9,11]. For other events, we obtained data from all nearby broadband stations and identified any aftershocks within a 2-day period following the mainshock. Any event showing P–S times similar to the mainshock was considered an aftershock. These aftershocks were added to any identified from the monthly Preliminary Determination of Epicenters (PDE) bulletin using the criteria noted above. If there were any appreciable aftershocks, the broadband data were searched for an additional time period. This procedure will identify any significant aftershock sequences, as the occurrence rate of aftershocks decays rapidly following the mainshock[9,12,13]. Because the deep earthquakes in this study vary in seismic moment by more than three orders of magnitude, the aftershock production must be corrected for differences in mainshock size. We normalize the number of aftershocks assuming that the number of aftershocks scale with M_w (ref. 5). The normalization simply permits results from a wider range of mainshock magnitudes to be compared simultaneously.

The results, when tabulated, suggest that aftershock production varies systematically between different subduction zones. Although there is substantial variability, the Tonga and Marianas subduction zones show more aftershocks on average than subduction zones in South America for deep earthquakes of equivalent size. Deep earthquakes in the Kurile, Japan, and Izu–Bonin regions also show few aftershocks.

Although the results shown in Fig. 1*a* have been normalized to permit comparison of a wide range of mainshock magnitudes, the differences in aftershock production are clear in the raw aftershock numbers. For example, the 1996 Indonesia event (M_w 7.8) in a relatively cold slab shows 14 aftershocks ($m_b \geq 4.5$), whereas the larger 1970 Colombia event (M_w 8.0) in a warm slab shows no aftershocks. The 1996 Indonesia event can also be compared to the 1973 Japan event (M_w 7.7) and the August 1963 Peru event (M_w 7.7), both of which occur in warmer slabs and also show no aftershocks. The 1994 Tonga event (M_w 7.6) in the coldest slab shows 19 aftershocks ($m_b \geq 4.5$), whereas the November 1963 Peru event with the same moment magnitude shows two aftershocks.

It may be thought that these trends reflect the detection levels in the various subduction zones. The converse is true, as detection levels in the Tonga and Marianas subduction zones are worse than in most other subduction zones. Of the subduction zones studied, the Tonga subduction zone shows one of the highest detection threshold levels, as indicated by changes in the slope of the magnitude–frequency curve. For example, only 60% of the $m_b \geq 4.5$ aftershocks from the 9 March 1994 Tonga event were detected by the PDE, as determined by comparison with the local broadband data.

Aftershock productivity shows a strong relationship to the thermal

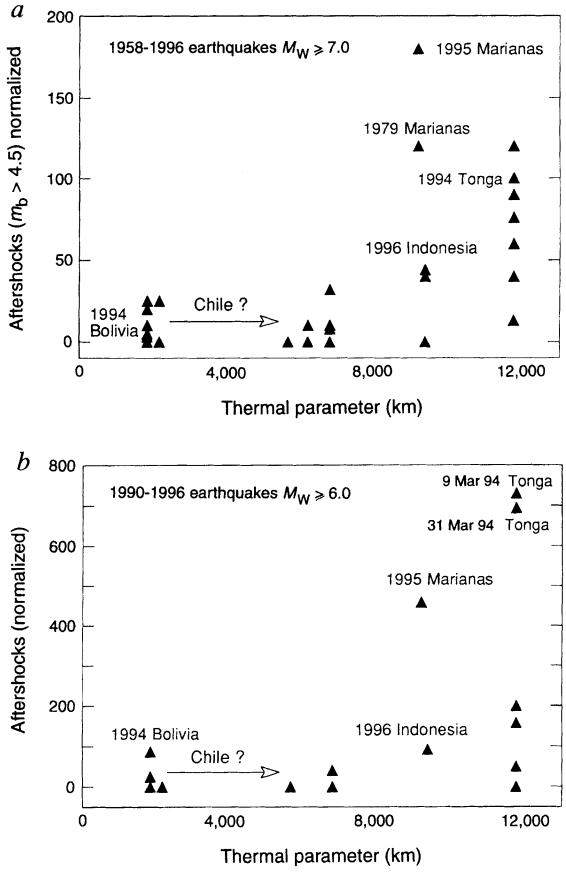

FIG. 1 *a*, Number of normalized aftershocks ($m_b \geq 4.5$) for large 1958–96 deep earthquakes (Table 1*a*) as a function of subduction-zone thermal parameter (product of vertical descent rate and the age of the subducting lithosphere). Larger thermal parameters correspond to cooler slabs. Uncertainty for the thermal parameter for Chile is shown by the arrow; thermal parameters as high as 6,500 km are possible if the deep seismic zone occurs within Mesozoic age lithosphere[16]. The number of aftershocks are normalized to correct for different mainshock sizes assuming that the logarithm of the number of aftershocks should be proportional to M_w, as is observed for shallow earthquakes. *b*, Total number of normalized aftershocks recorded for 1990–96 deep earthquakes (Table 1*b*) as a function of subduction-zone thermal parameter. Data is shown only for earthquakes for which the number of aftershocks could be checked by at least one broadband seismic station within 12° distance. Deep earthquakes in cold slabs show a much higher aftershock rate for both datasets.

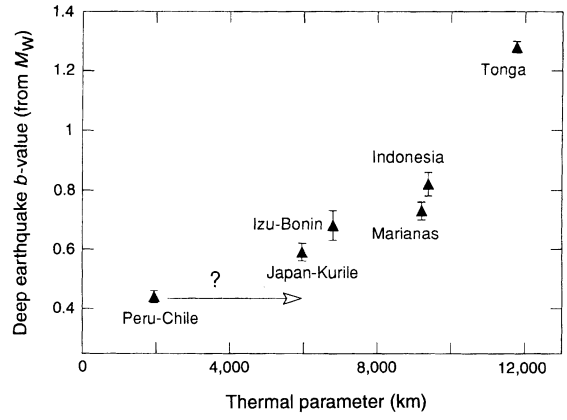

FIG. 2 The *b*-value determined from the magnitude–frequency relation for various deep seismic zones as a function of slab thermal parameter. The uncertainty for the thermal parameter of the Peru–Chile deep seismic zone is shown by the arrow. Cold deep seismic zones show a much higher *b*-value than warmer slabs, showing that larger earthquakes predominate in warmer slabs and demonstrating that the statistical behaviour of deep earthquakes is temperature dependent.

characteristics of the slab. Figure 1 plots the normalized number of aftershocks as a function of thermal parameter for both datasets. The thermal parameter, the product of the slab vertical-descent rate and the age of the subducting lithosphere, is a simple way of estimating the overall temperature structure of the deep slab. The use of the thermal parameter to compare temperatures at depth in the slab is justified theoretically if heating of the subducted lithosphere occurs by conduction and if the lithospheric temperature structure is given by a halfspace cooling model before subduction[14]. Larger thermal parameters correspond to cooler slab temperatures at depth. Table 2 lists the values used to calculate the thermal parameters for each subduction zone.

For several regions, some complicating factors must be taken into account in calculating the thermal parameter. The Tonga, Marianas and Izu–Bonin regions have active back-arc spreading systems, and so estimates of the back-arc spreading rate from marine surveys are added to the convergence rate of the major plates. Recent GPS surveys of the Tonga region[15] suggest an exceedingly fast convergence rate ($\sim$21 cm yr^{-1}). This rate is probably not indicative of the descent rate of the deep slab, so we use the absolute velocity of the Pacific plate to estimate the vertical descent rate of the steeply dipping deep part of the slab. For the South American subduction zones, uncertainty in the age of the lithosphere at depth complicates the calculation. It has been suggested that the material at depth may be as much as 100 Myr older than the currently subducting plate[16]. Plate reconstructions suggest that this is not the case for the deep seismic zone in the Peru region[17], but it is less clear for Chile. Use of the older lithospheric ages would raise the thermal parameter from about 2,200 to 6,500 km; the uncertainty in this parameter for Chile is shown by an arrow on the figures.

The maximum aftershock productivity is correlated with the slab thermal parameter for both datasets (Fig. 1). Deep earthquakes showing substantial aftershock productivity are limited to colder slabs, such as Tonga and the Marianas. Warmer slabs, such as Chile and Peru, consistently show few aftershocks. This suggests that the temperature of the slab plays a very important role in controlling

TABLE 1 Aftershocks of deep earthquakes

Date	Subduction zone	Depth (km)*	M_w†	Number‡	Normalized aftershocks§
a Aftershocks ($m_b \geq 4.5$) for 1958–96 deep earthquakes ($M_w \geq 7.0$)					
9 June 94	Bolivia	636	8.3	3	3
31 Jul 70	Colombia	651	8.0	0	0
17 Jun 96‖	Indonesia	565	7.8	14	44
15 Aug 63	Peru	543	7.7	0	0
29 Sep 73	Japan	575	7.7	0	0
26 Jul 58	Peru–Chile	650	7.6	1	5
9 Nov 63	Peru	600	7.6	2	10
9 Mar 94	Tonga	565	7.6	19	95
22 Jun 82	Indonesia	450	7.4	0	0
6 Mar 84	Izu–Bonin	457	7.4	1	8
7 Oct 68	Izu–Bonin	457	7.3	1	10
30 Aug 70	Kurile	645	7.3	1	10
21 Jul 94	Japan	473	7.3	0	0
31 Aug 61	Peru	626	7.2	2	25
9 Oct 67	Tonga	654	7.2	6	76
10 Feb 69	Tonga	673	7.2	1	13
11 Feb 69	Indonesia	450	7.2	0	0
30 Mar 72	Tonga	532	7.2	6	76
12 May 90	Kurile	611	7.2	0	0
23 June 91	Chile	581	7.2	2	25
8 Dec 62	Chile	620	7.1	0	0
29 Nov 74	Izu–Bonin	419	7.1	2	32
29 Jun 75	Japan	560	7.1	0	0
7 Mar 78	Izu–Bonin	442	7.1	0	0
26 May 86	Tonga	553	7.1	6	95
25 Aug 63	Tonga	557	7.0	2	40
15 Dec 63	Indonesia	650	7.0	0	0
23 Mar 74	Tonga	535	7.0	6	120
17 Oct 79	Marianas	601	7.0	6	120
16 June 86	Tonga	565	7.0	3	60
5 May 89	Peru	604	7.0	1	20
24 May 90	Indonesia	588	7.0	2	40
23 Aug 95	Marianas	595	7.0	9	180
b Aftershocks for 1990–96 deep earthquakes ($M_w \geq 6.0$)					
9 June 94	Bolivia	636	8.3	87	87
17 June 96‖	Indonesia	565	7.8	33	104
9 Mar 94	Tonga	565	7.6	144	722
21 Jul 94	Japan	473	7.3	0	0
23 Aug 95	Marianas	595	7.0	23	459
17 Oct 90	Peru	624	6.9	1	25
10 Jun 94	Peru	589	6.9	0	0
29 Apr 94	Chile	573	6.9	0	0
10 May 94	Chile	605	6.9	0	0
3 May 91	Izu–Bonin	459	6.7	1	40
20 Jun 92	Izu–Bonin	512	6.6	0	0
27 Oct 94	Tonga	549	6.6	1	50
19 Jan 93	Japan	455	6.5	0	0
31 Mar 94	Tonga	591	6.5	11	694
30 Oct 92	Isu–Bonin	406	6.4	0	0
19 Aug 94	Chile	565	6.4	0	0
17 Jan 95	Tonga	637	6.3	2	200
4 Nov 94	Peru	618	6.1	0	0
29 Oct 95	Tonga	611	6.1	1	158
19 Jan 94	Tonga	537	6.0	0	0

* Deep earthquakes are defined as deeper than 400 km for this study.

† Moment magnitude calculated from ref. 32 for 1958–61 earthquakes, from ref. 33 for 1962–76 earthquakes and from Harvard CMT solutions[34] for 1977–96 events.

‡ For *a* the number of aftershocks $m_b \geq 4.5$ from the Preliminary Determination of Epicenters (PDE) and the International Seismological Centre (ISC) are tabulated; for *b* the total number of aftershocks determined from all sources are tabulated. With the exception of 17 Jun 96, only events for which broadband waveform data was available from stations within 12° distance are included in *b*. The total number of aftershocks for 9 Mar 1994 are from ref. 10, and for 9 Jun 94 the number of aftershocks are taken from ref. 11.

§ Aftershocks are normalized assuming that the log of the number of aftershocks scales linearly with M_w. This relationship is consistent with aftershock sequences of shallow earthquakes in both California and Japan[26]. Aftershocks are normalized to the number expected for an M_w 8.3 earthquake using $\log N_n = 8.3 - M_w + \log N_o$, where N_n and N_o are the normalized and observed number of aftershocks respectively[5].

‖ Aftershock statistics for the recent 17 June 96 event are determined from the Reviewed Event Bulletin (REB) and the weekly PDE, as the monthly PDE data is not yet available. A magnitude correction is made to events located only by the REB. As no data are available from within 12°, the number of aftershocks for this event may be underestimated relative to the others in *b*.

TABLE 2 Subduction zone parameters

Subduction zone	Age (Myr)*	Velocity (mm yr^{-1})†	Backarc velocity‡	Angle (deg)§	Vertical velocity	Thermal parameter	b-value‖
Kurile	100	82	0	49	62	6,200	0.59 (± 0.03)
Japan	130	87	0	30	43	5,600	—
Izu-Bonin	145	55	5	51	47	6,800	0.68 (± 0.05)
Marianas	155	44	22	64	59	9,200	0.73 (± 0.03)
Indonesia	140	79	0	58	67	9,400	0.82 (± 0.04)
Tonga	110	84	130	53	107¶	11,800	1.28 (± 0.02)
Peru	41	78	0	35	44	1,800	0.44 (± 0.02)
Chile	45	84	0	35	48	2,200	—

* Age of the lithosphere entering the trench, from compilations of magnetic anomalies[35] and the magnetic timescale[36].
† Relative velocity at the trench[37].
‡ Backarc spreading rates taken from ref. 38 for the Marianas, ref. 39 for Izu–Bonin, and ref. 15 for Tonga.
§ Average slab dip, obtained by calculating the angle subtended by a line connecting the trench axis with the deep seismicity.
‖ Slope of the magnitude–frequency curve determined by least squares from 1977–95 M_w values (taken from the Harvard CMT catalogue[34] over an M_w range of 5.3–6.8. Adjacent subduction zones with similar thermal parameters were combined for the Peru–Chile and Japan–Kurile regions to obtain enough samples for the b-value determination. The uncertainty is the least-squares standard deviation.
¶Owing to slab rollback and the complex recent history of the Tonga slab, the vertical velocity is set to the absolute motion of the Pacific plate[40], to approximate the velocity of the descending slab relative to the mantle. Use of the complete convergence rate would result in a much larger thermal parameter.

the mode of seismic energy release in aftershock sequences, and that aftershock sequences may be particularly suppressed in warm sections of the slab. This observation is consistent with the characteristics of the large 1994 Tonga deep earthquake, which shows few aftershocks in the outermost, warmer region of the slab[8].

Previous studies have noted that deep earthquakes in different subduction zones show different slopes of the magnitude–frequency relation (b-value)[1,3–5]. We determined the b-values for the deep seismic zones studied here from a least-squares fit to 1977–95 M_w data, with M_w values determined from the Harvard centroid moment tensor (CMT) dataset. The Chile–Peru and Japan–Kurile regions were combined to obtain enough moment data to determine a b-value, as they are adjacent and have similar thermal parameters. The resulting b-values are also correlated with the thermal parameter (Fig. 2), suggesting that slab thermal structure also controls the magnitude–frequency relation for deep earthquakes. Not surprisingly, the subduction zones showing the largest b-values also tend to show greater aftershock activity[5]. A similar correlation is obtained using b-values determined from more numerous m_b data.

A previous study[4] has proposed that the difference in b-values between Tonga and other slabs is due to the effect of the finite width of slab material available for faulting, as has been observed for very large shallow earthquakes[18,19]. The present study shows that slab thermal structure significantly affects aftershock occurrence for equivalently sized faults. This effect cannot result from simple physical limits on the width of faults, which should not cause different aftershock levels for similar sized faults in different subduction zones. Rather, this study suggests a more fundamental effect of temperature on the statistics of deep earthquake faulting, including both magnitude–frequency relations and aftershock productivity.

Although some studies suggest small regions of anomalous magnitude–frequency relations at shallow or intermediate depth[20–22], shallow earthquakes generally show remarkably uniform b-values[3,23]. Similarly, although some differences in aftershock and foreshock production have been reported for shallow events[24,25], other studies find shallow aftershocks consistently proportional to fault area[26], and no systematic aftershock production anomalies have been definitively established[13]. This study demonstrates that aftershock production and magnitude–frequency relations for deep earthquakes are temperature dependent in a fundamentally different way from shallow earthquakes.

The observation that deep earthquake statistical properties are temperature dependent provides important constraints on deep-earthquake generating processes. Several proposed mechanisms for deep earthquakes are expected to be highly temperature sensitive, beyond the obvious temperature effect of limiting slab width. One possible candidate is plastic shear instabilities[27,28], which are likely to be highly temperature dependent. These instabilities may be triggered in the slab core by transformational faulting[29–31]. □

Received 4 May; accepted 1 October 1996.

1. Giardini, D. *J. Geophys. Res.* **93,** 2095–2105 (1988).
2. Frohlich, C. *Annu. Rev. Earth Planet. Sci.* **17,** 227–254 (1989).
3. Frohlich, C. & Davis, S. D. *J. Geophys. Res.* **98,** 631–644 (1993).
4. Okal, E. A. & Kirby, S. H. *Phys. Earth Planet. Inter.* **92,** 169–187 (1995).
5. Wiens, D. A. & McGuire, J. J. *Geophys. Res. Lett.* **22,** 2245–2248 (1995).
6. Kirby, S. H., Stein, S., Okal, E. A. & Rubie, D. *Rev. Geophys.* **34,** 261–306 (1996).
7. Green, H. W. I. & Houston, H. *Annu. Rev. Earth Planet. Sci.* **24,** 169–213 (1995).
8. McGuire, J. J., Wiens, D. A., Shore, P. J. & Bevis, M. G. *J. Geophys. Res.* (in the press).
9. Wiens, D. A. *et al. Nature* **372,** 540–543 (1994).
10. Wiens, D. A., McGuire, J. J. & Shore, P. J. *J. Geophys. Res.* (in the press).
11. Myers, S. C. *et al. Geophys. Res. Lett.* **22,** 2269–2272 (1995).
12. Davis, S. D. & Frohlich, C. *J. Geophys. Res.* **96,** 6335–6350 (1991).
13. Kisslinger, C. *Adv. Geophys.* **38,** 1–36 (1996).
14. Molnar, P., Freedman, D. & Shih, J. S. F. *Geophys. J. R. Astron. Soc.* **56,** 41–54 (1979).
15. Bevis, M. *et al. Nature* **374,** 249–251 (1995).
16. Engebretson, D. E. & Kirby, S. (abstr.) *Eos* **87,** 33–54 (1994).
17. Okal, E. A. & Bina, C. R. *Phys. Earth Planet. Inter.* **87,** 33–54 (1994).
18. Pacheco, J. F., Scholz, C. H. & Sykes, L. R. *Nature* **355,** 71–73 (1992).
19. Okal, E. A. & Romanowicz, B. A. *Phys. Earth Planet. Inter.* **87,** 55–76 (1994).
20. Weimer, S. & Benoit, J. P. *Geophys. Res. Lett.* **23,** 1557–1560 (1996).
21. Mori, J. & Abercrombie, R. (abstr.) *Eos* **76,** 388 (1995).
22. Anderson, R. N., Hasegawa, A., Umino, N. & Takagi, A. *J. Geophys. Res.* **85,** 1389–1398 (1980).
23. Rundle, J. B. *J. Geophys. Res.* **94,** 12337–12342 (1989).
24. Singh, S. K. & Suarez, G. *Bull. Seismol. Soc. Am.* **78,** 230–242 (1988).
25. Abercrombie, R. E. & Mori, J. *Nature* **381,** 303–307 (1996).
26. Yamanaka, Y. & Shimazaki, K. *J. Phys. Earth* **38,** 305–324 (1990).
27. Ogawa, M. *J. Geophys. Res.* **92,** 13801–13810 (1987).
28. Hobbs, B. E. & Ord A. *J. Geophys. Res.* **93,** 10521–10540 (1988).
29. Kirby, S. H. *J. Geophys. Res.* **92,** 13789–13800 (1987).
30. Green, H. W. & Burnley, P. C. *Nature* **341,** 733–737 (1989).
31. Green, H. W., Young, T. E., Walker, D. & Scholz, C. H. *Nature* **348,** 720–722 (1990).
32. Abe, K. *J. Phys. Earth* **30,** 321–330 (1982).
33. Huang, W.-C., Okal, E. A., Ekstrom, G. & Salganik, M. P. *Phys. Earth Planet. Inter.* (in the press).
34. Dziewonski, A. M., Chou, T.-A. & Woodhouse, J. H. *J. Geophys. Res.* **86,** 2825–2852 (1981).
35. Cande, S. C. *et al. Magnetic Lineations of the World's Ocean Basins* (Am. Assoc. Petroleum Geologists, Tusla, OK, 1989).
36. Harland, W. B. *et al. A Geologic Time Scale – 1989* (Cambridge Univ. Press, 1990).
37. DeMets, C., Gordon, R. G., Argus, D. F. & Stein, S. *Geophys. J. Int.* **101,** 425–478 (1990).
38. Hussong, D. M. & Uyeda, S. *Init. Rep. DSDP Leg* 909–929 (1991).
39. Taylor, B. *et al. J. Geophys. Res.* **96,** 16113–16129 (1991).
40. Gripp, A. E. & Gordon, R. G. *Geophys. Res. Lett.* **17,** 1107–1112 (1990).

ACKNOWLEDGEMENTS. We thank J. McGuire and B. Park-Li for assistance in the early stages of this project, and W.C. Huang and E.A. Okal for results before publication. Some of the results reported here came from the Southwest Pacific Seismic Experiment, which used equipment from the PASSCAL program of the incorporated Research Institutions in Seismology (IRIS). Global data were obtained from the IRIS Data Management Center. This research was supported by the US National Science Foundation.

CORRESPONDENCE should be addressed to D.A.W. (doug@kermadec.wustl.edu)